

# NEW Fe I LEVEL ENERGIES AND LINE IDENTIFICATIONS FROM STELLAR SPECTRA

Ruth C. Peterson

SETI Institute and Astrophysical Advances, 607 Marion Pl, Palo Alto, CA 94301

e-mail: [peterson@ucolick.org](mailto:peterson@ucolick.org)

Robert L. Kurucz

Harvard-Smithsonian Center for Astrophysics, 60 Garden Street, Cambridge, MA 02138

*Short title:* New Fe I Identifications from Stellar Spectra

## ABSTRACT

The spectrum of the Fe I atom is critical to many areas of astrophysics and beyond. Measurements of the energies of its high-lying levels remain woefully incomplete, however, despite extensive analysis of ultraviolet laboratory iron absorption spectra, optical laboratory iron emission spectra, and the solar infrared spectrum. In this work we use as sources the high-resolution archival absorption-line ultraviolet and optical spectra of stars, whose warm temperatures favor moderate Fe I excitation. We derive the energy for a particular upper level in Kurucz's semiempirical calculations by adopting a trial value that yields the same wavelength for a given line predicted to be about strong as that of a strong unidentified spectral line observed in the stellar spectra, then checking the new wavelengths of other strong predicted transitions that share the same upper level for coincidence with other strong observed unidentified lines. To date this analysis has provided the upper energies of 37 Fe I levels. Many new level energies are higher than those accessible to laboratory experiments; several exceed the Fe I ionization energy. These levels provide new identifications for over a thousand potentially detectable lines. Almost all of the new levels of odd parity include UV lines that were detected but unclassified in laboratory Fe I absorption spectra, providing an external check on the energy values. We motivate and present the procedure, provide the resulting new level energies and their uncertainties, list all the potentially detectable UV and optical new Fe I line identifications and their gf-values, and discuss the prospects for additional Fe I energy-level determinations in the near future.

*Key words:* atomic data – line: identification – methods: laboratory: atomic – stars: individual (HD 29139, HD 72660, HD 76932, HD 85503, HD 94028, HD 124897, HD 140283, HD 157466, HD 160617, HD 165341, HD 184499, HD 211998, HD 217107) – techniques: spectroscopic – ultraviolet: stars

## 1. INTRODUCTION

Astrophysical research has dramatically gone forward in the last two decades, fueled by rapid advances in key areas. Telescopes and detectors are larger, and make increasingly precise observations of progressively fainter and more distant objects. The analysis of these datasets has surged due to exponentially increasing capabilities of computers and networked systems.

Lagging far behind are the laboratory astrophysics data necessary to interpret this information. These are the fundamental physical parameters that characterize the spectral absorption and emission of the atomic and molecular systems that pervade stars, stellar nebulae, exploding supernovae, and the interstellar and intergalactic medium, from the local environment to the highest redshifts.

Line parameters for the iron atom are a particularly important case. While energy levels, wavelengths, and transition probabilities (gf-values) can often be theoretically derived for light, simple atoms, there is no substitute for determining empirically the energy levels of an atom as complex and as abundant as iron. Because lines of neutral iron dominate the solar absorption spectrum, especially over 1500Å – 2100Å where they outnumber Fe II and Si I lines by a factor of five (Tousey 1988), Fe I has been investigated extensively in the laboratory and from the solar spectrum itself.

Summarizing previous work, Nave & Johansson (1993b) derived energies from laboratory spectra for 86 new Fe I levels, from which Nave & Johansson (1993a) identified and established wavelengths for over 2000 Fe I lines from 1700Å to 5μm. Nonetheless, Nave & Johansson (1993b) conclude: “In the ultraviolet below 3000Å, 650 lines have been identified in the laboratory spectra, of which 600 correspond to solar features. The UV solar spectrum below 2095Å has been extensively studied by Moore, and almost all of the 87 solar lines in our list have already been identified by her. Clearly many more solar lines in this region are also due to Fe I, and originate from still higher levels than the ones reported here.”

A similar situation prevails in the infrared. To reach Fe I levels with energies from 59000 cm<sup>-1</sup> to 61700 cm<sup>-1</sup>, Johansson et al. (1994) and Schoenfeld et al. (1995) analyzed Fe I supermultiplets in the solar infrared spectrum, identifying nearly 200 lines in three IR windows 35, 6, and 40 cm<sup>-1</sup> wide. These new IR Fe I lines are weak, usually with depths less than 10% of the solar continuum (Johansson et al. 1994, Fig. 5). They form a small minority compared to the unidentified lines remaining in the Hinkle et al. (1995) infrared spectrum of the metal-poor red giant Arcturus. Although Arcturus has an iron abundance three times lower than that of the Sun (e.g. Peterson et al. 1993), many of these unidentified IR lines are strong: Table 6 of Hinkle et al. (1995) lists 72 unidentified lines whose depths are 10% or more in the infrared Arcturus spectrum.

Currently, most of the Fe I lines that remain unidentified fall either in the UV, from 1500Å to 4000Å, or in the infrared, beyond 1μm. Those in the UV are transitions between known low-lying levels to high, still-unmeasured upper levels; those in the infrared are transitions between high levels, one or both of which is unmeasured. Addressing this semiempirically, Kurucz (2011) ran calculations that extrapolate experimentally-determined energy values to unknown energy levels and predict the associated wavelengths. His website currently provides results from such comprehensive calculations for all iron-peak elements. However, because wavelengths are fixed by the difference in energy levels, wavelengths of predicted lines are usually in error, typically by 10Å or more near 2000Å, and by much more in the infrared.

## 2. THE NEED FOR NEW Fe I LINE IDENTIFICATIONS

Several areas of astronomy are severely impacted by unidentified Fe I lines. Among them are the determinations of abundances for trace elements in individual stars from their UV spectra (e.g. Peterson 2011, 2013), with the potential to unravel the nucleosynthesis processes and environments in which the earliest stars and their heavy elements were formed (Sneden et al. 2008). Identified infrared lines and their gf-values are vital (Ruffoni et al. 2013) for infrared spectroscopic iron abundances of luminous red giants in dust-obscured regions like the bulge, bar, and disk of the Milky Way plus the Sagittarius stream (SDSS III/APOGEE: Majewski et al. 2010). All across the spectrum, new line identifications are needed to fill significant poorly-modeled gaps in spectra of stars of solar metallicity and temperature, improving the fidelity of theoretical models of UV (Peterson et al. 2002) and blue (Coelho 2014) spectral energy distributions (SEDs).

Fe I identifications will assist efforts using SEDs or panchromatic photometry to discriminate low metallicity from young age in globular clusters (HST PHAT: Dalcanton et al. 2012) and galaxies of moderate redshift (Carnegie-Spitzer-IMACS: Kelson et al. 2014), especially in heavy reddening. Newly identified Fe I lines in the 3000Å – 4000Å region will aid the flurry of recent detailed interpretations of optical spectra of nearby extragalactic globular clusters and galaxies. Age and overall metallicity can then be more accurately derived (Conroy 2013), improving deduced self-enrichment (Schiavon et al. 2013), abundances of lighter and heavier elements (Conroy, Graves, & van Dokkum 2014) and galactic assembly histories at low redshifts (Choi et al. 2014; SLUGGS: Brodie et al. 2014). Interpretations of galaxies in deep photometric surveys (HST Frontier Fields/JWST: <http://www.stsci.edu/hst/campaigns>) will benefit from analogous improvements in UV modeling, for example to characterize interloping galaxies at redshifts  $1 < z < 3$  (e.g. Hayes et al. 2012), where the rest-frame UV is redshifted into the well-observed optical and near-IR.

Although the observations of distant clusters and galaxies are not at high resolution themselves, to disentangle physical parameters such as metallicity and age, most rely on prior high-resolution templates (e.g. UVBLUE: Rodriguez-Merino et al. 2005). The near-UV flux distribution of light versus wavelength of turnoff stars is the primary tool for deriving metallicity and age of old, distant stellar systems from their integrated light. Only in the near-UV do turnoff stars dominate, and can their temperatures provide an age. But the weaker near-UV line blanketing of metal-poor turnoff stars mimics the intrinsically bluer near-UV flux of hotter, younger, more metal-rich stars. Near-UV fluxes need high-resolution templates for discriminating metallicity and age. Even in the optical, significant corrections are needed to spectral calculations for stars of solar type and cooler to give reliable SEDs. Coelho (2014, Fig. 3) shows that at high metallicities, the problem is significant bluer than 5000Å for solar-temperature stars, and is serious throughout the optical for cool giants, whose fluxes dominate those of dwarfs redward of 4300Å in old elliptical galaxies (Worthey 1994, Fig. 41). Coelho (2014) provide functional corrections that should be useful for wavelengths beyond 2800Å (their Fig. 5).

Efforts to address this problem in the UV with HST Treasury program GO-9455 have been stymied by the increasing numbers of unidentified lines towards bluer wavelengths and the increasing strength of these lines towards higher metallicity. The severity of the problem in the near-UV is seen in Figure 1, adapted from Peterson et al. (2002). This compares observed spectra of one hot and six near-turnoff stars whose metallicities range from 1/100 solar to slightly supersolar ( $-2.0 \leq [\text{Fe}/\text{H}] \leq +0.15$ ). Observed stellar near-UV fluxes (heavy lines) are superimposed on theoretical spectra (light lines) that Peterson, Dorman, & Rood (2001) calculated, specifically leaving out the Kurucz predicted lines. Including them alleviates the flux deficiency but compromises the spectrum match.

The hot, low-metallicity blue horizontal branch star at the top stands out due to its high temperature. Indeed, our modeling has provided useful diagnostics for the presence of such stars in globular clusters (GCs; Peterson et al. 2003), thus clarifying the age of nearby systems with  $[\text{Fe}/\text{H}] < -1.5$  that are older than  $\sim 1$  Gyr. As Brodie et al. (2014) note, their inclusion is especially necessary now that “helium-enriched blue horizontal branches are probably very common ... [to distinguish them from] populations of young GCs.”

Crippling the modeling of the UV spectra of solar-temperature stars is the problem illustrated in Fig. 1. As temperature drops and metallicity increases, flux is increasingly underestimated in regions not dominated by strong absorption lines. The underestimate reaches a factor of three at solar metallicity in the 2650Å – 2720Å region. This is the most likely source of the sudden increase below 2800Å in the discrepancy seen in Fig. 5 of Coelho (2014) between their high-resolution calculations and SEDs. Likewise our calculations are not reliable enough at near-solar metallicity to provide the critical

diagnostics that can separate the effects of metallicity and temperature on spectra of stars like the Sun. This is unfortunate, because the widely-used, high-resolution, 850 – 4700Å UVBLUE theoretical spectral templates (Rodriguez-Merino et al. 2005), incorporated into the Koleva & Vazdekis (2012) assessment of the HST/STIS Next Generation Spectral Library (Gregg et al. 2006), were also calculated without the Kurucz predicted lines.

Below 2300Å, matters only become worse. Peterson (2011) turned to archival E230H STIS spectra near 2000Å to establish in metal-poor turnoff stars the abundances of light trans-ironic elements using strong near-UV lines. Only by guessing identifications of unidentified absorption features redward of 2000Å, Peterson (2011) surprisingly found molybdenum and ruthenium to be very overabundant – by up to an order of magnitude – in two moderately metal-poor turnoff stars, with  $[Fe/H] = -1.4$  and  $-1.8$ . However, the Peterson (2011) figures show the same trend continuing at bluer wavelengths as is seen in the 2300Å – 3140Å region of Figure 1. As metallicity increases, unidentified lines begin to swamp the fluxes, badly compromising both the continuum and the blending in spectra of turnoff stars even at 1/30 solar metallicity,  $[Fe/H] = -1.4$ . According to Brodie et al. (2014), about three-quarters of extragalactic GCs have metallicities higher than this, as do all but the very outermost stars of their host elliptical galaxies – the ones so rarely included in age and metallicity determinations.

### 3. IDENTIFYING Fe I LINES AND LEVELS FROM STELLAR SPECTRA

To remedy this, in our HST Cycle 21 AR-13263 program we have undertaken the identification of these lines in metal-poor turnoff stars directly from their ultraviolet spectra. We first established that unidentified lines are overwhelmingly due to Fe I. This was seen by running calculations over 1600Å – 8900Å that included only the Kurucz (2011) predicted lines of all neutral species plus Fe II, covering FGK stars in the temperature range 4000K – 6500K. These lines are present in the observed spectra, but have unknown wavelength offsets in the computed spectra.

We then began to empirically establish upper-level energies for Fe I from the same five archival HST E230H echelle spectra of Peterson (2011), by matching modified predictions to the positions of their unidentified absorption lines. Our procedures are similar to those followed by Castelli & Kurucz (2010) to identify 109 high levels of Fe II from the optical spectrum of a slowly-rotating B star. The energy difference between the upper and lower levels of a transition fixes its wavelength, and in the UV nearly all lower levels have energies found in the laboratory. Thus we adopt a trial energy by shifting the wavenumber for a specific predicted level to match the predicted and observed wavenumbers of a near-UV line that the Kurucz predictions suggest is as strong as an observed but unidentified spectral line. We then check the wavenumbers of the other strong predicted lines that share the same upper level for coincidence with other strong observed unidentified lines. Matching positions exactly and gf-values approximately for four or more transitions with same upper level confirms its energy. Other lines of the same multiplet will have similar shifts, so their starting guesses become closer.

A critical aspect of this program is the interplay between new identifications and subsequent predictions. Each new level identification and energy value better constrain the Fe I atomic matrix calculations that produce the predicted lines. Once Peterson has found a number of new levels, Kurucz incorporates these into his computation of the Fe I matrix, described just below. The new energy values strongly constrain levels of similar structure whose energies remain unknown, improving their wavelength predictions for Peterson’s next Fe I search.

Predicted energy levels and log gf values were computed by Kurucz with his version of the Cowan (1981) code (Kurucz 2009). The calculation included the 61 even configurations  $d^6 4s^2$ ,  $d^6 4s 5s$ – $10s$ ,

$d^6 4s 4d-10d$ ,  $d^6 4s 5g-9g$ ,  $d^6 4s 7i-9i$ ,  $d^6 4s 9l$ ,  $d^8$ ,  $d^7 4s-10s$ ,  $d^7 4d-10d$ ,  $d^7 5g-9g$ ,  $d^7 7i-9i$ ,  $d^9 9l$ ,  $d^5 4s^2 5s-10s$ ,  $d^5 4s^2 4d-10d$ , and  $d^6 4p^2$  with 18655 levels least-squares fitted to 442 known levels. The 50 odd configurations included  $d^6 4s 4p-9p$ ,  $d^6 4s 4f-9f$ ,  $d^6 4s 6h-9h$ ,  $d^6 4s 8k-9k$ ,  $d^7 4p-10p$ ,  $d^7 4f-9f$ ,  $d^7 6h-9h$ ,  $d^7 8k-9k$ ,  $d^5 4s^2 4p-9p$ , and  $d^5 4s^2 4f-9f$  with 18850 levels least-squares fitted to 559 known levels. The calculations were done in LS coupling with all configuration interactions included, with scaled Hartree-Fock starting guesses, and with Hartree-Fock transition integrals. A total of 7498208 lines were saved from the transition array, of which 101763 lines are between known levels and have good wavelengths.

Deriving an energy for a particular Fe I level establishes the identifications and wavelengths for all transitions that share this level and also arise from a known lower level, regardless of its energy and thus its wavelength. Thus a slew of lines from the UV through the IR may be solved in a single level. Because the upper energy remains fixed, the lower energy of this series of transitions increases steadily towards the red. The lower levels of UV Fe I transitions are already known, because they are all low. They are influential absorbers even at gf-values of  $-3$ , because Boltzmann excitation in warm stars still favors the low levels. Those of moderate excitation are more easily detected in such 6000K stars than in the Brown et al. (1988)  $\sim 2000$ C iron furnace. The drawback: many stellar Fe I lines are blended by lines of other elements.

#### 4. STELLAR SPECTRA AND ANALYSIS

Panchromatic stellar spectra are critical to this identification procedure, to increase the number of lines for a given level against which a match can be found, since lines that share the same upper level are spread over wavelengths from 1600Å to 6μm and beyond. Furthermore, as wavelength increases, line profiles become steadily narrower in wavelength space, reducing the uncertainty in the deduced energy levels. However, at progressively longer wavelengths, Fe I line strengths are diminished by the lower Boltzmann populations as the lower energy level steadily rises towards the red. Consequently, spectra of progressively stronger-lined stars were adopted at redder wavelengths, culminating in stars of solar-metallicity and higher and solar temperatures or lower as wavelengths approached 1μm. In the infrared, Nave & Johansson (1993a) note that “the best source for Fe I is the Sun”.

Table 1 summarizes the spectra adopted. Below the stellar names are the model parameters  $T_{\text{eff}}$ ,  $\log g$ , and  $[\text{Fe}/\text{H}]$  used for the calculations. The spectral characteristics include the spectrograph, wavelength coverage, the data reduction procedure or the source from which reduced spectra were downloaded, and the exposure times. The sources include StarCat (Ayres 2010), the UVES and HIRES pipelines, and the UVES ground-based spectral programs of the Next Generation Spectral Library (NGSL; Gregg et al. 2006). All spectra are of intrinsically sharp-lined stars obtained at resolutions of  $\sim 60,000$  in the UV, and 40,000 – 80,000 or better in the optical. Signal-to-noise ratios S/N exceed 50 for all spectra except below 2000Å. S/N greatly exceeds this for the best-observed optical spectra, those of the Sun and the metal-poor K giant Arcturus. They were obtained with the Fourier Transform Spectrometer (FTS) and coudé feed spectrograph at Kitt Peak; all the others are echelle grating spectra.

In the optical, we have relied very heavily on the Kurucz (2005) solar flux spectrum and the Hinkle et al. (2000) Arcturus atlas. We also have made use of the  $R = 80,000$ ,  $S/N > 200$  spectrum of the K5 giant  $\alpha$  Tau, obtained for the stellar parameter workshop of Lebzelter et al. (2012). The  $\sim 1500$ K temperature difference between giants and solar-type stars allows us to better discern the plausible values of the lower excitation potential from the difference in the strength of an unknown line in giants versus solar-type stars. For the ground-based near-UV and blue, we have added archival spectra over a wide metallicity range from VLT/UVES (e.g. Bagnulo et al. 2003) and Keck/HIRES with upgraded UV sensitivity (Vogt et al. 1994). The high quality of the latter and our ability to reproduce them

synthetically is seen in the figures of Peterson (2013), who derived abundances for light trans-ironic elements from the 3050Å – 4000Å region of the HIRES spectra of metal-poor dwarfs that Boesgaard et al. (2011) obtained for Be II lines near 3130Å.

Conversely, progressively more metal-poor stars were included as wavelength decreases. This is essential to reduce line blending, notably the crowding of the unidentified Fe I lines among themselves. Those from odd-parity levels dominate below 2300Å, and blend so strongly with one another below 1935Å that Brown et al. (1988) could identify only a handful. To minimize this blending, which is significant even at the lowest stellar metallicities available, we added HD 72660, a metallic-lined A star to isolate the very strongest unidentified Fe I lines. Lines from even-parity levels similarly converge near 2500Å, since odd-parity levels from which even-parity levels must arise have their lowest energies near 19500 cm<sup>-1</sup>. This is too high for the furnace of Brown et al., who detected virtually none. In stars of solar temperature, blending is again severe above 1/100 solar metallicity, [Fe/H] = -2.

All but one of the space-based UV spectra were obtained with the E230H echelle grating of the Space Telescope Imaging Spectrograph (STIS). In the mid-UV, for the Hubble Treasury program GO-9455 such spectra were obtained for sharp-lined stars of types sdB, A, F, G, and K, some at 60,000 resolution out to 3150Å. Peterson (2008) illustrates how well our calculations match spectra at 3065Å of the metal-poor turnoff stars HD 184499 and HD 157466, with ( $T_{\text{eff}}$ , log  $g$ , [Fe/H]) = (5750K, 4.1, -0.5) and (6050K, 4.3, -0.45), as well as the solar-metallicity F5 IV standard Procyon and the Sun itself. The UV spectra near 2000Å were taken primarily for boron abundances (e.g. Thorén & Edvardsson 2000).

## 5. SPECTRAL SYNTHESIS METHODS

Peterson generates stellar spectra using an updated version of the Kurucz (1993) program SYNTHE. Input is a list of molecular and atomic line transitions with wavelengths, energy levels, and laboratory and computed gf-values (revised to match the stellar line strengths), and a static, one-dimensional model stellar photosphere of effective temperature  $T_{\text{eff}}$ , gravity log  $g$ , overall metallicity [Fe/H], and microturbulent velocity  $v_t$ . These parameters are derived exclusively from the spectra, not colors.  $T_{\text{eff}}$  is derived as noted just below, [Fe/H] from iron lines, and  $v_t$  and log  $g$  from trends with line strength or ionization, plus the breadth of wings of strong lines. As reported by Peterson, Dorman, & Rood (2001), a consistent determination of the stellar temperature emerges from all available diagnostics. These always include demanding the same abundances be deduced from low- and high-excitation lines of the same species, and that the wings of the profiles of Balmer lines be reproduced. If space-based ultraviolet spectra are on hand, we also match mid-UV flux levels and the continuum slope of the mid-UV spectrum. The Balmer wings agree with other  $T_{\text{eff}}$  diagnostics only when convective overshoot is turned off. We thus use Castelli & Kurucz (2003) ODFNEW models, which also adopt an improved solar iron abundance and continuum and line opacities.

We use an input line list that we have improved by comparing calculations to echelle spectra of a wide variety of standard stars. This includes lines identified in the laboratory, but not lines whose wavelengths or identifications are unknown. Moving from weak-lined to stronger-lined stars, we calculate each spectrum, then adjust gf-values singly for atomic lines and as a function of band and energy for molecular lines. We revise and recalculate until all spectra match. These LTE calculations fit both optical and mid-UV spectra of a wide range of metal-poor and solar-metallicity standard stars (Peterson 2005, 2008, 2011, 2013).

Any nonLTE effects are expected to be small for the range in temperature, metallicity, and gravity of the stars considered here (Table 1), according to Lind et al. (2012). Their Fig. 2 shows that the nonLTE

effect expected on our Fe I abundances never exceeds 0.1 dex. Similarly, from their Fig. 6, the nonLTE effect on  $T_{\text{eff}}$  values derived from Fe I excitation, such as ours, is 30K or less. Lind et al. (2012) find that their results for Fe I nonLTE effects “are in good quantitative agreement with those of Mashonkina et al. (2011)” but are of smaller size than in earlier works in which the numerous high-lying Fe I levels of the Kurucz (2007) expanded Fe I calculations were not included. They note: “Mashonkina et al. (2011) demonstrated in detail how recent developments in atomic data calculations have improved the NLTE modeling of iron lines. In particular, R. L. Kurucz’s calculations of high excitation energy levels beyond reach of experiments have enabled a realistic coupling to the next ionization state.”

## 6. ILLUSTRATIONS OF THE LINE IDENTIFICATION PROCEDURE

Figures 2 – 5 illustrate the identification of a single level via four of its least-blended transitions. Progressing from the ultraviolet redward, each figure includes a line whose upper level is 5.0 (4F)6p 3G, at  $59357.03 \text{ cm}^{-1}$ . These lines are at  $47380.79 \text{ cm}^{-1}$  (2108.89Å; Fig. 2),  $33005.99 \text{ cm}^{-1}$  (3028.87Å; Fig. 3),  $22311.10 \text{ cm}^{-1}$  (4480.82Å; Fig. 4), and  $11396.01 \text{ cm}^{-1}$  (8772.53Å, Fig. 5). Each plot compares observed and calculated spectra for several stars. Their identifications are given at left, along with the effective temperature  $T_{\text{eff}}$ , gravity  $\log g$ , metallicity [Fe/H], and microturbulent velocity  $v_t$  of the atmospheric model, derived as described above. Observed spectra are in blue. Calculations that include the new line identifications are in red; those lacking them, in black.

The ultraviolet region near 2110Å in Figure 2 shows two strong newly-identified lines and illustrates the high quality of five archival STIS E230H spectra. In Figure 3, the region near 3030Å shows three new identifications, all moderately strong. The HD 140283 spectrum shows the value of high S/N, bringing out very weak unidentified lines that grow substantially below. Only one new weak line is seen in Figure 4. This shows ground-based spectra near 4480Å of generally stronger-lined stars. The star HD 184499 at the bottom of Fig. 3 is now found at the top of Fig. 4, and spectra of the Sun, the super-metal-rich giant  $\mu$  Leo, and the metal-poor giant Arcturus appear at the bottom. The other two stars are a solar-metallicity dwarf and a metal-rich turnoff star. Figure 5 shows the near-IR region near 8770Å. Weak-lined stars are dropped, and the cool giant  $\alpha$  Tau is substituted for  $\mu$  Leo due to the excellent quality of its spectrum (Lebzelter et al. 2012).

In each figure the new identifications stand out: the red line is deeper than the black. The calculated and observed positions of the four 5.0 (4F)6p 3G lines all coincide, confirming our result for its energy value. Each newly-identified line is well reproduced in all stars. Moreover, the strengths of the new lines match regardless of stellar temperature. The two reddest 5.0 (4F)6p 3G lines illustrate this well. The line at 4480.82Å in Fig. 4 is stronger in Arcturus than in the Sun, but the line at 8772.53Å in Fig. 5 is stronger in the Sun than in Arcturus. The former has a value of  $37045.93 \text{ cm}^{-1}$  for its lower excitation potential, while the latter has a high value of  $47960.94 \text{ cm}^{-1}$ . Taken together, the figures also illustrate the general trend for both known and unidentified lines to become weaker towards the red.

## 7. RESULTS TO DATE

In this way we have now matched four or more transitions in 37 levels with energies up to  $67716 \text{ cm}^{-1}$ . In so doing we have identified more than a thousand individual lines over  $1600\text{Å} - 5.4\mu\text{m}$  that are strong enough to be detected in warm and cool stars of moderate to high metallicity, of which more than a third are in the infrared. There are 870 lines from  $1680\text{Å}$  to  $9000\text{Å}$  with  $\log gf > -3$ , and 369 lines redward with  $\log gf > -2$ . The transitions whose energies are most easily established are those with strong lines in well-observed, uncrowded regions (e.g. Figs 2, 4). These form the majority of the levels we have successfully identified to date.

Thanks to the UV spectra, and to the high quality of the solar and Arcturus optical spectra, this approach reaches higher Fe I energies than any previous work, reaching a maximum at  $67716 \text{ cm}^{-1}$ . Five levels have energies higher even than the Fe I ionization potential of  $63737.7 \text{ cm}^{-1}$  (Schoenfeld et al. 1995). Table 2 lists separately for the newly-identified even and odd levels the full and abbreviated labels and J-value of each new level, and the associated energy and its uncertainty in wavenumbers. Table 3 provides a wavelength-ordered list of the newly-identified UV and optical lines. For each line sufficiently strong and unblended that the gf-value could be estimated to  $\pm 0.2$  dex, Table 3 includes an entry for dgf, the log gf-value from spectral matching minus the predicted log gf-value.  $\Gamma_{\text{R}}$  is the logarithm of the radiative damping constant.  $\Gamma_{\text{S}}$  is the logarithm of the Stark damping constant / electron number density per  $\text{cm}^3$ .  $\Gamma_{\text{W}}$  is the logarithm of the van der Waals damping constant / neutral hydrogen number density per  $\text{cm}^3$ . The same information for IR lines will be forthcoming once we have extended the spectral synthesis to wavelengths redward of  $9000\text{\AA}$ .

We have estimated the uncertainty in each individual energy determination from visual inspection of the goodness of fit of every reasonably-unblended line. Our values range from  $0.01$  to  $0.1 \text{ cm}^{-1}$ , generally higher than the Nave & Johansson (1993a) uncertainty of  $0.01 \text{ cm}^{-1}$ . Since line profiles are broader at short wavelengths, as noted above, our uncertainties depend strongly on the distribution in wavelength of the subset of lines sufficiently unblended to constrain the energy.

Confirmation of our energy values is available for 18 levels of odd parity. These have three or more strong UV lines whose wavenumbers Brown et al. (1988) determined but could not classify. For many such lines they were able to assign an energy and J value; 14 of our 18 levels have these assignments, and our results always agree. The difference in the average of the 18 level energies between our work and theirs is  $0.045 \pm 0.032 \text{ cm}^{-1}$ . The latter is similar to the  $0.042 \text{ cm}^{-1}$  rms value Schoenfeld et al. (1995) found in identifying infrared Fe I lines from the solar spectrum.

Serendipitous confirmation that the line at  $5382.263\text{\AA}$  is due to a high-excitation transition, whose upper level we ascribe to the even-parity level  $6.0 \text{ 4s3H5s 5H}$  at  $64300.51 \text{ cm}^{-1}$ , is provided by Fig. 1 of Wallace et al. (2011). This compares the solar disk-center spectrum with the solar flux spectrum in the region near  $5380\text{\AA}$ . Of the several weak lines depicted, only the unidentified  $5382.26\text{\AA}$  line shows the deeper core and narrower profile in the disk-center spectrum that is also seen in the C I line at  $5380.32\text{\AA}$ . This behavior is due to the very high lower excitation potentials of these two lines,  $45726.13 \text{ cm}^{-1}$  for the Fe I line and  $61981.82 \text{ cm}^{-1}$  for the C I line. The disk-center spectrum views the Sun directly from above, and looks deeper into its hot layers.

## 8. FUTURE PROSPECTS

Due to the very high data quality of the solar spectra, thousands of potentially detectable lines are available for many of the remaining unidentified levels, for levels of both even and odd parity. Over two thousand of these are in the infrared. From existing solar spectra we expect to identify hundreds more Fe I levels, and are beginning with new f, g, h, and i levels. In the UV, should additional spectra become available, hundreds of additional unknown Fe I levels could be found that have few strong lines outside the UV. These include levels with moderately weak lines scattered throughout the UV, and levels of odd parity with several strong lines below  $1930\text{\AA}$  but few beyond.

Each set of new identifications is submitted for publication at the same time that Kurucz updates all the Fe I material on his website, including the new energy levels, line identifications, predicted gf-values, and gf-values derived from the stellar spectra. In this way, the entire community engaged in solving the



astrophysical problems in Sec. 1 is able to freely access and use these improvements immediately.

We thank Richard Monier for suggesting HD 72660 as a target and providing the far UV data, J. X. Prochaska for his reductions of the Keck HIRES data, and D. Silva and R. Hanuschik for the reduced UVES NGSL spectra. Support for this work under program number HST-AR-13263 was provided by NASA through a grant from the Space Telescope Science Institute, which is operated by the association of Universities for Research in Astronomy, Inc. under NASA contract NAS 5-26555. Ground-based spectra are largely based on observations made with ESO Telescopes at the Paranal Observatory with the UVES spectrograph under programs 065.L-0507(A), 072.B-0585(A), and 266.D-5655(A), and with the Keck Observatory HIRES spectrograph, under programs H6aH (PI A. Boesgaard), N01H, N12H, and N13H (PI D. Latham), U17H and U63H (PI J. Prochaska), U35H (PI A. Wolfe), and U44H (PI M. Rich). This research has made use of the Keck Observatory Archive (KOA), which is operated by the W. M. Keck Observatory and the NASA Exoplanet Science Institute (NExScI), under contract with the National Aeronautics and Space Administration. Space-based spectra are based on observations made with the NASA/ESA Hubble Space Telescope under GO programs 7348, 7402, 8197, 9146, 9455, 9491, and 9804. These data were obtained from the HST and StarCat archives hosted by the Mikulski Archive for Space Telescopes (MAST). IRAF is distributed by the National Optical Astronomy Observatories, which are operated by the Association of Universities for Research in Astronomy, Inc., under cooperative agreement with the National Science Foundation.

## REFERENCES

- Ayres, T.R. 2010, *ApJS*, 187, 149
- Bagnulo, S., Jehin, E., Ledoux, C., Cabanac, R., et al. 2003, *ESO Messenger*, 114, 10
- Boesgaard, A. M., Rich, J. A., Levesque, E. M., & Bowler, B. P. 2011, *ApJ*, 743, 140
- Brodie, J.P., Romanowsky, A.J., Strader, J., Forbes, D.A., Foster, C., Jennings, Z.G., Pastorello, N., Pota, V., et al. 2014, *ApJ*, submitted; arXiv:1405.2079
- Brown, C.M., Ginter, M.L., Johansson, S., & Tilford, S.G. 1988, *JOSA B*, 5, 2125
- Castelli, F., & Kurucz, R.L. 2003, *IAU Symp. No 210*, “Modeling of Stellar Atmospheres”, eds. N. Piskunov et al., CD-ROM poster A20; also astro-ph 0405087; ODFNEW models are at <http://kurucz.harvard.edu/grids/> and <http://wwwuser.oat.ts.astro.it/castelli/grids.html>
- Castelli, F., & Kurucz, R.L. 2010, *A&A*, 520, 57
- Choi, J., Conroy, C., Moustakas, J., Graves, G.J., Holden, B.P., Brodwin, M., Brown, M.J.I., & van Dokkum, P.G. 2014, *ApJ*, submitted; arXiv:1403.4932
- Coelho, P.R.T. 2014, *MNRAS* 440, 1027
- Conroy, C. 2013, *ARA&A*, 51, 139
- Conroy, C., Graves, G.J., & van Dokkum, P.G. 2014, *ApJ*, 780, 33
- Cowan, R.D. 1981, *The Theory of Atomic Structure and Spectra*, Los Alamos Series in Basic and Applied Sciences, Berkeley, University of California Press
- Dalcanton, J.J., Williams, B.F., Lang, D., Lauer, T.R., Kalirai, J.S., et al. 2012, *ApJS* 200, 18.
- Gregg, M.D., Silva, D., Rayner, J., et al. 2006, in “The 2005 HST calibration workshop: Hubble after the transition to two-gyro mode” (eds. A.M. Koekemoer, P. Goudfrooij, and L.L. Dressel), NASA/CP2006-214134, 209.
- Hayes, M., Laporte, N., Pello, R., Schaerer, D., & LeBorgne, J.-F. 2012, *MNRAS*, 425, 19
- Hinkle, K., Wallace, L., Livingston, W. 1995, “Infrared Atlas of the Arcturus Spectrum 0.9 – 5.3 $\mu$ m” (ASP: San Francisco)
- Hinkle, K., Wallace, L., Valenti, J., & Harmer, D. 2000, “Visible and Near Infrared Atlas of the Arcturus Spectrum 3727 – 9300Å” (ASP: San Francisco)

- Johansson, S., Nave, G., Geller, M., Sauval, A.J., Grevesse, N., Schoenfeld, W.G., Change, E.S., & Farmer, C.B. 1994, ApJ 429, 419
- Kelson, D.D., Williams, R.J., Dressler, A., McCarthy, P.J., et al. 2014, ApJ 783, 110
- Koleva, M., & Vazdekis, A. 2012, A&A, 538, 143
- Kurucz, R.L. 1993, CD-ROM 18, SYNTHE Spectrum Synthesis Programs and Line Data (Cambridge: Smithsonian Astrophys. Obs.); at <http://kurucz.harvard.edu/>
- Kurucz, R.L. 2005, Kitt Peak Solar Flux Atlas; at <http://kurucz.harvard.edu/sun/fluxatlas2005>
- Kurucz, R.L. 2007, in *The 9<sup>th</sup> International Colloquium on Atomic Spectra and Oscillator Strengths (ASOS9)*, ed. G.M. Wahlgren, W.L. Wiese, & P. Beiersdorfer, J. Phys.: Conf. Ser. 130.
- Kurucz, R.L. 2009, Am. Inst. Phys. Conf. Ser., 1171, 43
- Kurucz, R.L. 2011, Can. J. Phys., 89, 417
- Lebzelter, T., Heiter, U., Abia, C., Eriksson, K., Ireland, M., Neilson, H., Nowotny, W., Maldonado, J., Merle, T., Peterson, R., et al. 2012, A&A, 547, 108
- Lind, K., Bergemann, M., & Asplund, M. 2012, MNRAS 427, 50
- Majewski, S.R., Wilson, J.C., Hearty, F., Schiavon, R.P., & Skrutskie, M.F. 2010, IAU Symp. 265, 480
- Mashonkina, L., Gehren, T., Shi J.-R., Korn, A.J., & Grupp, F., 2011, A&A 528, A87
- Nave, G., & Johansson, S. 1993a, A&A 274, 961
- Nave, G., & Johansson, S. 1993b, A&AS 102, 269
- Peterson, R.C. 2005, Hubble 2005 Science Year in Review, ed. H. Ferguson (NASA/STScI)
- Peterson, R.C. 2008, Space Telescope Sci. Inst. Newsletter, 25, no. 1 (Spring 2008), p. 24
- Peterson, R.C. 2011, ApJ, 742, 21
- Peterson, R.C. 2013, ApJ, 768, L13
- Peterson, R.C., Carney, B. W., Dorman, B., Green, E. M., Landsman, W., Liebert, J., O’Connell, R.W., & Rood, R.T. 2002, in the Proceedings of the NASA Laboratory Astrophysics Workshop, ed. F. Salama et al., 73
- Peterson, R.C., Carney, B. W., Dorman, B., Green, E. M., Landsman, W., Liebert, J., O’Connell, R.W., & Rood, R.T. 2003, ApJ, 588, 299
- Peterson, R.C., Dalle Ore, C.M., & Kurucz, R.L. 1993, ApJ, 404 333
- Peterson, R.C., Dorman, B., & Rood, R.T. 2001, ApJ, 559, 372
- Rodriguez-Merino, L. H., Chavez, M., Bertone, E., & Buzzoni, A. 2005, ApJ, 626, 411
- Ruffoni, M.P., Allende Prieto, C., Nave, G., & Pickering, J.C. 2013, ApJ 779, 17
- Schiavon, R.P., Caldwell, N., Conroy, C., Graves, G.J., Strader, J., MacArthur, L.A., Courteau, S., & Harding, P. 2013, ApJ 776, 7
- Schoenfeld, W.G., Change, E.S., Geller, M., Johansson, S., et al. 1995, A&A, 301, 583
- Snedden, C., Cowan, J.J., & Gallino, R. 2008, ARA&A, 46, 241
- Thorén, P., & Edvardsson, B. 2000, A&A 363, L33
- Tousey, R. 1988, JOSA B, 5, 2230
- Vogt, S. S., Allen, S. L., Bigelow, B. C., et al. 1994, in Society of Photo-Optical Instrumentation Engineers (SPIE) Conference Series, 2198, ed. D. L. Crawford & E. R. Craine, 362
- Wallace, L., Hinkle, K.H., Livingston, W.L., & Davis, S.P. 2011, ApJS, 195, 6
- Worthey, G. 1994, ApJS 95, 107

TABLE 1

## Stellar Parameters and Spectra

Star, Model	Wavelength (Å)	Instrument	Program	Reduction	T (ks)
Sun 5775 4.40 +0.00	2960 – 13000	NSO FTS		Kurucz (2005)	
HD 29139 ( $\alpha$ Tau) 3950 1.10 +0.00	4900 – 9750	2m NARVAL at Pic du Midi	U. Heiter	Lebzelter et al. (2012)	
HD 72660 9525 4.00 +0.35	1630 – 1902 2129 – 2888 3022 – 5845	STIS 230H STIS 230H HIRES	GO 9146 GO 9455 U17H	Monier IRAF Prochaska	1.65 1.64 0.15
HD 76932 5900 4.10 -1.00	1880 – 2150 3022 – 4975	STIS 230H UVES	GO 9804 266.D-5655(A)	StarCat 53054-53056 Pipeline	23.86 0.34
HD 85503 ( $\mu$ Leo) 4650 2.70 +0.40	5582 – 5665 5578 – 8560	HIRES HIRES	U44H U63H	Pipeline + IRAF Pipeline + IRAF	0.01 0.06
HD 94028 6050 4.30 -1.40	1880 – 2150 2278 – 3120 3050 – 4989	STIS 230H STIS 230M UVES	GO 8197 GO 7402 072.B-0585(A)	IRAF IRAF NGSL	33.05 0.60 0.75
HD 124897 (Arcturus, $\alpha$ Boo) 4275 1.30 -0.55	3727 – 9300	Coudé Feed  KPNO 0.9m	Hinkle et al.  Table 3	Hinkle et al. (2000)	
HD 140283 5400 3.60 -2.60	1950 – 2300 2378 – 2891 2885 – 3147 3080 – 5953	STIS E230H STIS E230H STIS 230H HIRES	GO 7348 GO 9455 GO 9491 U35H	StarCat uvsum2126 IRAF StarCat 52831-52844 Prochaska	18.32 5.28 62.57 0.60
HD 157466 6050 4.30 -0.45	2378 – 3158 3085 – 3996	STIS 230H HIRES	GO 9455 U35H	IRAF Prochaska	11.11 1.26
HD 160617 6000 3.80 -1.80	1880 – 2150 3057 – 3873 4400 – 6780	STIS 230H UVES HIRES	GO 8197 65.L-0507(A) H6aH	StarCat 51480-51787 Pipeline Extracted	39.39 3.00 0.42
HD 165341 5300 4.50 +0.00	3736 – 10425	UVES	71.B-0529(A)	Pipeline	0.05
HD 184499 5750 4.10 -0.50	2378 – 3159 3847 – 4986	STIS 230H HIRES	GO 9455 N01/N12/N13H	IRAF Pipeline + IRAF	11.26 0.18
HD 211998 5300 3.30 -2.60	1880 – 2150 3040 – 10400	STIS 230H UVES	GO 9804 266.D-5655(A)	IRAF Pipeline	29.40 0.60
HD 217107 5600 4.20 +0.30	3750 – 10252	UVES	076.B-0055(A)	Pipeline	0.33

TABLE 2

## New Fe I Levels and Energies

Expanded Label	Label	J	E (cm <sup>-1</sup> )	$\sigma$ (cm <sup>-1</sup> )
<i>17 Even Levels:</i>				
3d6 4s(6D)4d e7F	4s6D4d e7F	0	51143.92	0.03
3d7(4F)4d 5D	(4F)4d 5D	0	54304.21	0.02
3d6 4s(6D)4d 5D	4s6D4d 5D	0	58428.17	0.03
3d6 4s(4D)4d 5P	4s4D4d 5P	1	58628.41	0.03
3d7(4P)5s 3P	(4P)5s 3P	1	59300.54	0.03
3d7(4F)5d 5F	(4F)5d 5F	2	59366.79	0.02
3d7(2F)4s 1F	(2F)4s 1F	3	38602.26	0.02
3d6 4s(4D)4d 3G	4s4D4d 3G	3	59294.42	0.02
3d7(2G)5s 3G	(2G)5s 3G	3	61724.84	0.01
3d7(2G)5s 3G	(2G)5s 3G	4	61340.46	0.01
3d7(2G)5s 1G	(2G)5s 1G	4	61935.47	0.01
3d6 4s(3H)5s 5H	4s3H5s 5H	4	64531.78	0.03
3d7(2G)5s 3G	(2G)5s 3G	5	61198.49	0.01
3d7(2H)5s 1H	(2H)5s 1H	5	66293.98	0.01
3d7(2G)4d 3I	(2G)4d 3I	5	67687.99	0.01
3d6 4s(3H)5s 5H	4s3H5s 5H	6	64300.51	0.02
3d7(2G)4d 1I	(2G)4d 1I	6	67716.75	0.01
<i>20 Odd Levels:</i>				
d7(2P)4p 1S	(2P)4p 1S	0	55179.91	0.08
d6(3P)4s4p(3P) 1P	3Psp3P 1P	1	50675.08	0.05
d7(4F)7p 5D	(4F)7p 5D	2	61866.45	0.05
d7(4F)6p 5D	(4F)6p 5D	3	59089.65	0.03
d6(3P)4s4p(3P) 1F	3Dsp3P 1F	3	59794.85	0.03
d7(4F)6p 3G	(4F)6p 3G	3	60013.27	0.05
d6(5D)4s(6D)7p 5F	4s6D7p 5F	3	60055.93	0.05
d7(4F)7p 3G	(4F)7p 3G	3	62016.99	0.10
d7(4F)7p 5G	(4F)7p 5G	3	62287.54	0.10
d7(4F)8p 3D3G3F	8p 3D3G3F	3	62509.75	0.04
d7(4F)6p 5D	(4F)6p 5D	4	58729.80	0.08
d7(4F)6p 5G	(4F)6p 5G	4	59377.30	0.02
d6(5D)4s(6D)7p 5D	4s6D7p 5D	4	59496.62	0.05
d7(4F)6p 3G	(4F)6p 3G	4	59731.29	0.05
d7(4F)7p 5F	(4F)7p 5F	4	61678.26	0.05
d7(4F)8p 3G5G5F	8p 3G5G5F	4	62683.77	0.05
d7(4F)6p 5G	(4F)6p 5G	5	59021.31	0.06
d7(4F)6p 3G	(4F)6p 3G	5	59357.03	0.02
d7(4F)7p 5F	(4F)7p 5F	5	61155.95	0.05
d6(3G)4s4p(1P) 3G	3Gsp1P 3G	5	62107.29	0.05

Note. The three largest eigenvector components for each level can be found in the log files from the least squares fits, b2600e.log and b2600o.log, on the Kurucz website [kurucz.harvard.edu/atoms/2600](http://kurucz.harvard.edu/atoms/2600).

TABLE 3

## Newly Classified Lines of Fe I

Wavelength (nm)	log gf	d <sub>gf</sub>	E <sub>even</sub> (cm <sup>-1</sup> )	J <sub>e</sub>	Label <sub>e</sub>	E <sub>odd</sub> (cm <sup>-1</sup> )	J <sub>o</sub>	Label <sub>o</sub>	Γ <sub>R</sub>	Γ <sub>S</sub>	Γ <sub>W</sub>
160.5458	-3.244	...	0.000	4	4s2 a5D	62287.54	3	(4F)7p 5G	7.76	-3.71	-6.99
160.5966	-3.584	...	415.933	3	4s2 a5D	62683.77	4	8p 3G5G5F	8.30	-3.23	-7.02
161.0117	-2.644	...	0.000	4	4s2 a5D	62107.29	5	3Gsp1P 3G	8.32	-2.99	-7.03
161.0466	-3.849	...	415.933	3	4s2 a5D	62509.75	3	8p 3D3G3F	8.28	-3.80	-7.03
161.2461	-2.754	...	0.000	4	4s2 a5D	62016.99	3	(4F)7p 3G	8.12	-3.24	-7.09
161.6250	-2.142	...	415.933	3	4s2 a5D	62287.54	3	(4F)7p 5G	7.76	-3.71	-6.99
161.7973	-2.839	...	704.007	2	4s2 a5D	62509.75	3	8p 3D3G3F	8.28	-3.80	-7.03
162.1317	-1.924	...	0.000	4	4s2 a5D	61678.26	4	(4F)7p 5F	7.60	-3.47	-7.02
162.3349	-2.660	...	415.933	3	4s2 a5D	62016.99	3	(4F)7p 3G	8.12	-3.24	-7.09
162.3811	-3.275	...	704.007	2	4s2 a5D	62287.54	3	(4F)7p 5G	7.76	-3.71	-6.99
163.2325	-2.752	...	415.933	3	4s2 a5D	61678.26	4	(4F)7p 5F	7.60	-3.47	-7.02
163.4990	-3.234	...	704.007	2	4s2 a5D	61866.45	2	(4F)7p 5D	7.70	-3.59	-7.06
163.5164	-1.960	-0.20	0.000	4	4s2 a5D	61155.95	5	(4F)7p 5F	7.10	-4.19	-7.06

Note. Table 3 is published in its entirety in the electronic edition of The Astrophysical Journal. A portion is shown here for guidance regarding its form and content.

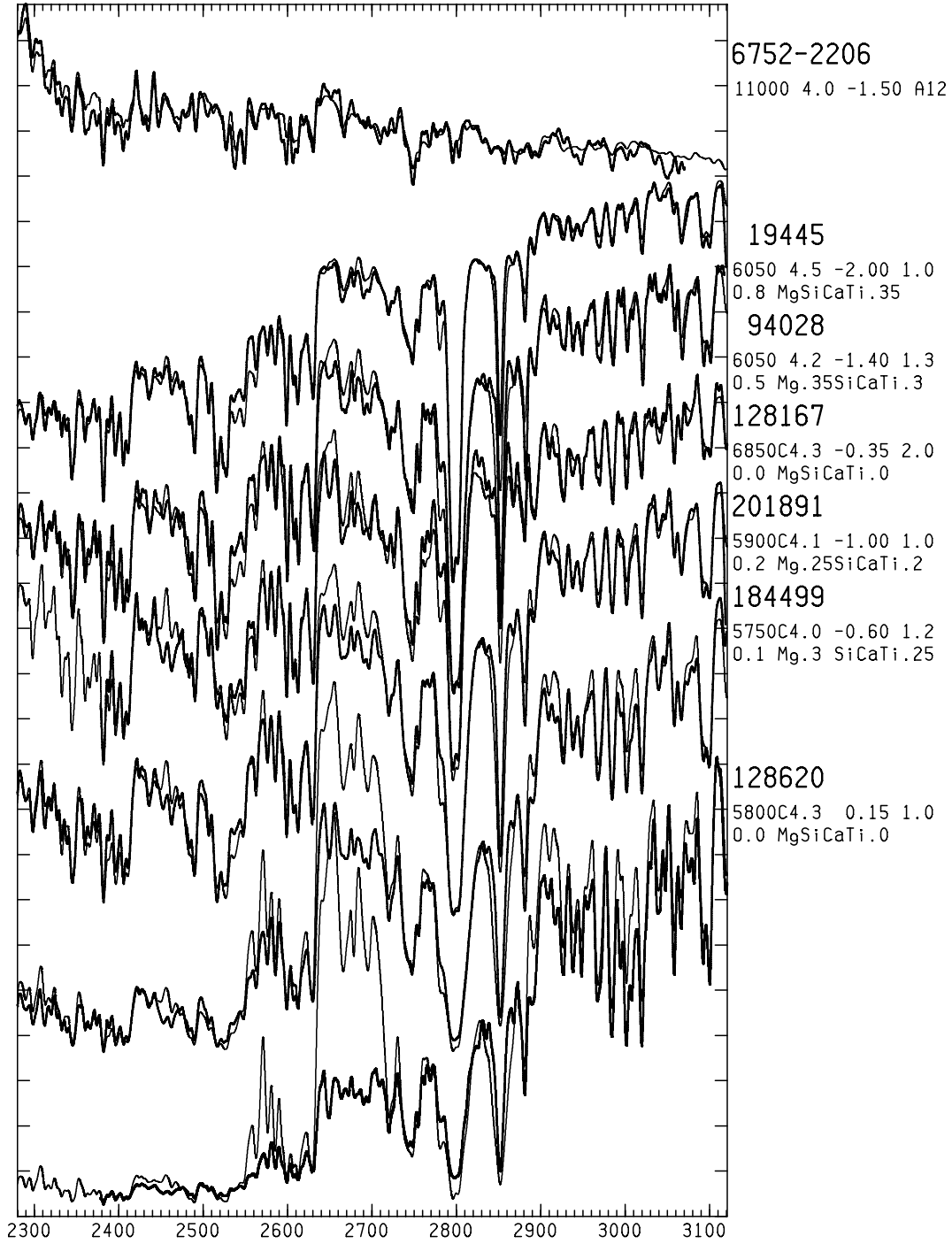


Figure 1 – Comparisons are shown of spectral calculations (light lines) to observations (heavy lines) for six metal-poor stars plus  $\alpha$  Cen A. Their HD numbers and model parameters appear at the right. Each stellar comparison is vertically offset; Y-axis ticks represent 10% of full scale. Wavelengths in Å appear at the bottom. Adapted from Peterson et al. (2002).

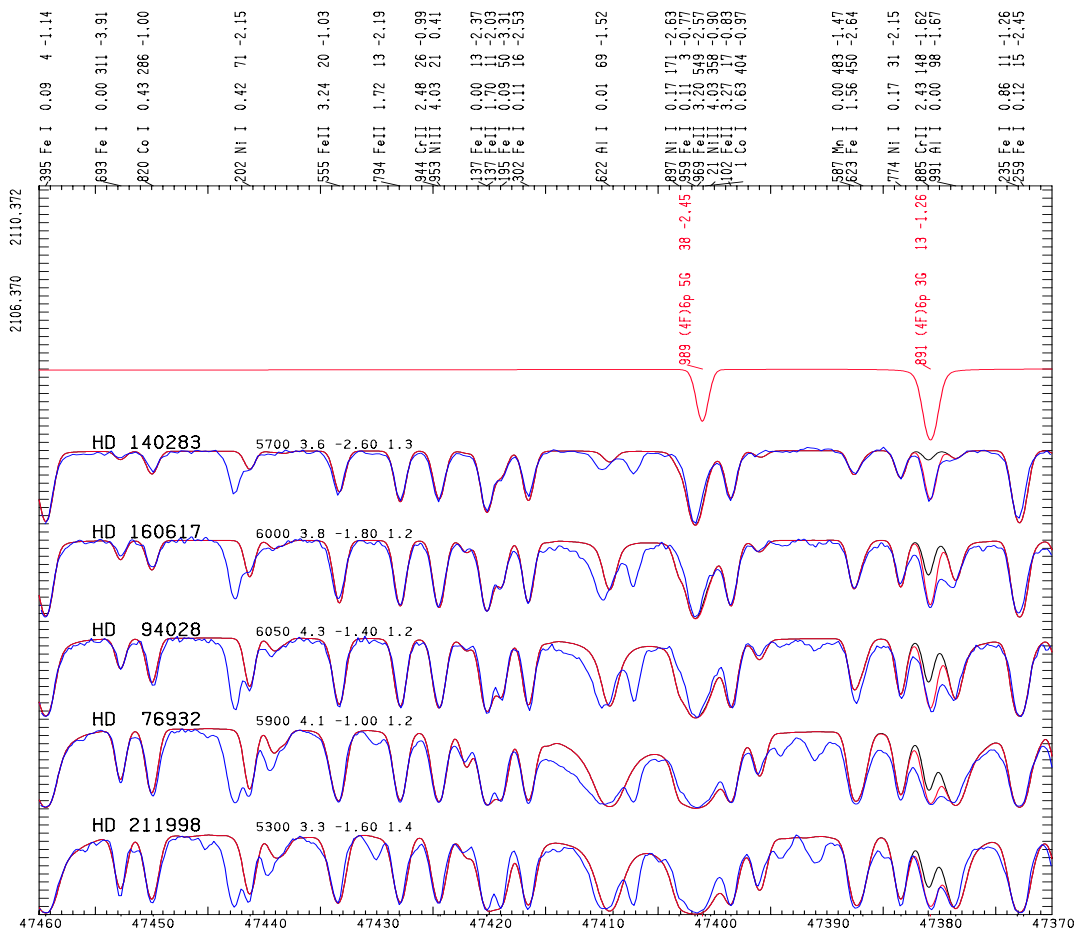


Figure 2 – Comparisons are shown in the 2110Å region between the observed and calculated spectra for five metal-poor stars. The stellar identification is on the left with the parameters  $T_{\text{eff}}$ ,  $\log g$ ,  $[\text{Fe}/\text{H}]$ , and  $v_t$ , the temperature, gravity, overall metallicity and microturbulent velocity adopted for the model atmosphere. Wavenumbers in  $\text{cm}^{-1}$  appear at the bottom. The wavelength range in Å of the plot is given at upper left. Strong lines are identified at the top. First are the digits following the decimal place of the line center wavelength in Å (in air  $> 2000\text{Å}$ ). Next are the species giving rise to the line, the lower excitation of the line in eV, an indicator of its strength (stronger lines have smaller numbers), and its  $\log gf$ -value. Blue lines are observations, which are HST STIS spectra below 3050Å and ground-based in the optical. Black and red lines are spectral calculations. The black line lacks the newly-identified Fe I lines; the red line includes them. Only the new lines were included in the top calculation.

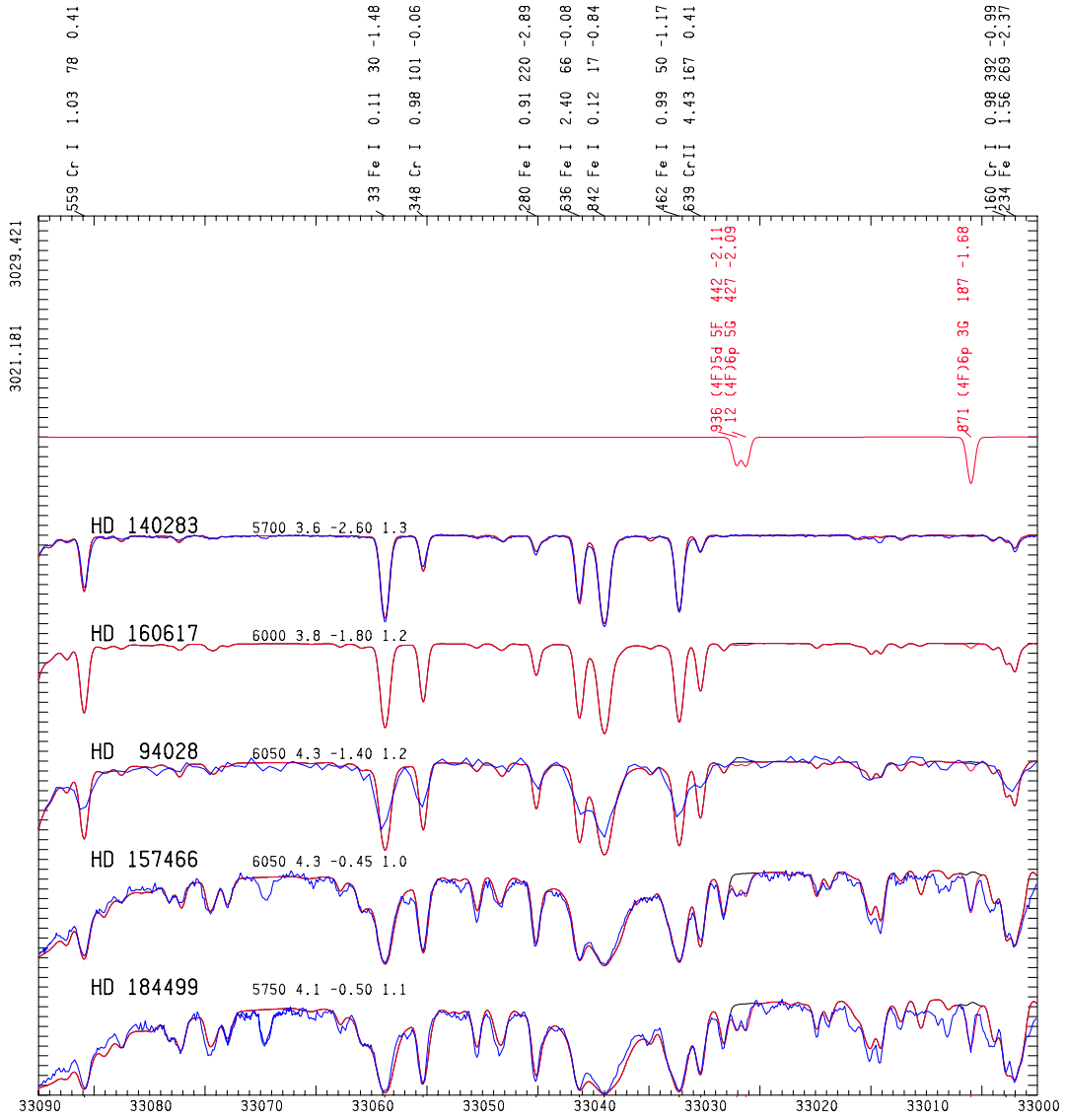


Figure 3 – Comparisons like those in Figure 2 are shown for stars in the 3025 Å region.



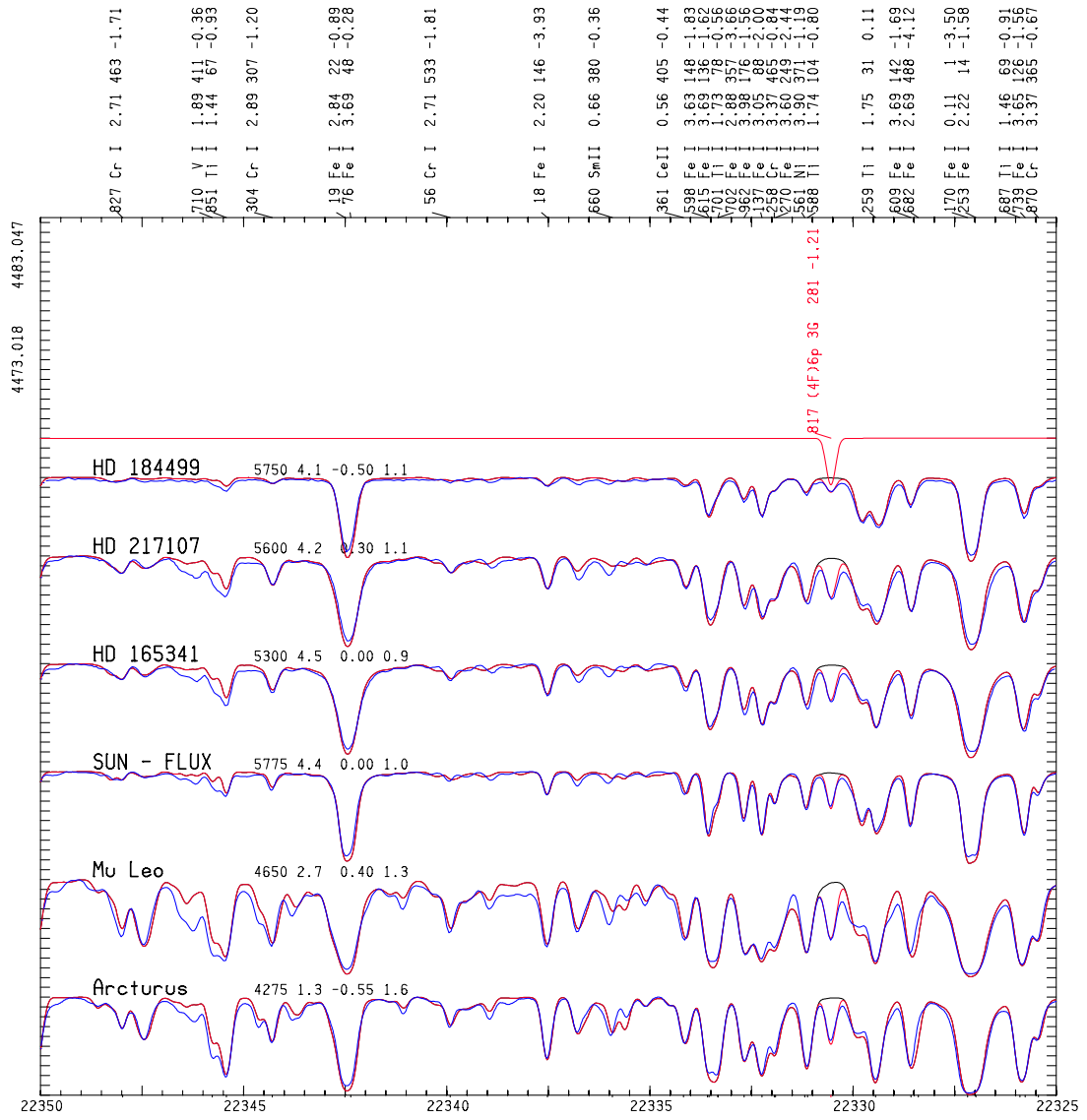


Figure 4 – Comparisons like those in Figure 2 are shown for five stars in the 4480 Å region.

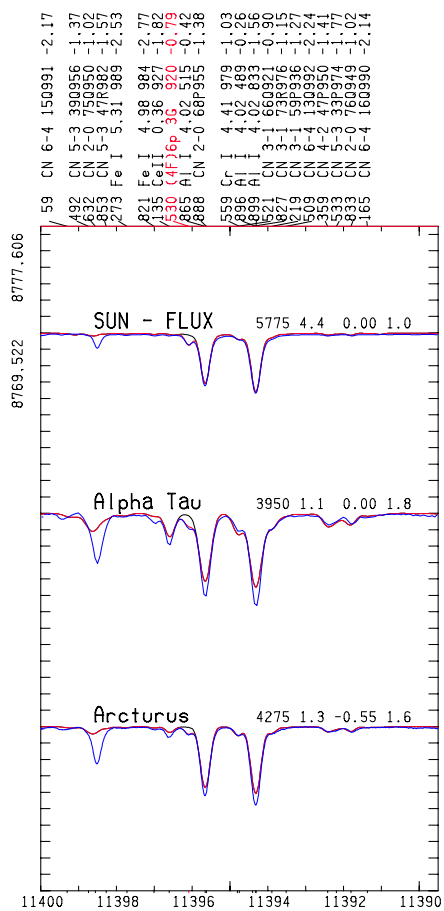


Figure 5 – Comparisons like those in Figure 2 are shown for three stars in the 8770Å region. The single newly-identified Fe I line in this region appears at 8772.53Å.